MICROMECHANICAL FEM MODELING OF THERMAL STRESSES IN FUNCTIONALLY GRADED MATERIALS

S. Akbarpour, H. R. Motamedian, A. Abedian
Aerospace Engineering Department, Sharif University of Technology

Keywords: *Functionally Graded Material (FGM) - Micromechanical Modeling- Finite Element Method (FEM) - CoCrAlY/Zro$_2$*

Abstract

The most common use of FG materials is as barrier coating against large thermal gradients. Thermal stresses in FG materials, if not released, may cause structural discontinuities in outer surfaces or even inside the material such as cracks, debonding, etc. In this research work, using Finite element method and micro-mechanical modeling of FG thermal barrier coatings, stresses under thermal and mechanical loadings of the same and different phases have been investigated. Also, the effect of some parameters such as refinement and offsetting of particles on stresses are studied. As for the loading, thermal cycle and in-phase and out-of-phase thermo-mechanical cyclic loadings are considered. The material is assumed to be CoCrAlY/Zro$_2$ where the volume fraction of Zro$_2$ in CoCrAlY is assumed to vary linearly through the thickness. With applying appropriate boundary conditions, the stress state in X-dir at different time steps are found.

1 Introduction

Functionally graded materials (FGMs) are ideal candidates for applications that involve sever thermal gradients, ranging from thermal structures in advanced aircraft and aerospace engines to computer circuit boards. In fact, this type of application was the original motivation for developing this class of materials.

Due to the difference between the Coefficient of Thermal Expansion (CTE) of the FGM constituents, large thermal stresses form inside these materials. Such stresses may then cause discontinuity like cracks and interface debonding or large inelastic deformation that may reduce load carrying capacity of the material. For instance, the crash of space shuttles in recent years is somehow attributed to the insufficient knowledge about the behavior of their FGM Thermal Barrier Coatings (TBCs) in high temperature environments or their response to the in-phase and out-of-phase thermo-mechanical loads.

2 Previous Research Works

Many macro-mechanical research works regarding the thermal stress and deformation analysis of FGMs would be found in the literature [1-6]. In these studies normally a power law or exponential variation for the material properties is assumed and the material response is calculated by different techniques like Gaussian numerical integration along the thickness or the Veronui cell finite element. However, in the present research work the response of these materials to a thermal environment is investigated from the micro-mechanical point of view. One of the rare studies using micro-mechanical modeling is the work done by Arnold et al. [7], where a two-dimensional higher-order theory was used for calculating the stress fields in FGMs. However, the formulation used in the study is very complicated and no follow up has been proposed or considered so far. For avoiding the complications involved, here in this study the FEM approach in conjunction with three micro-mechanical models is used for thermal stress analysis of FGMs. Fig. 1 presents the results that Arnold et al. [7] obtained.

In the Arnold et al. research work the temperature-dependent inelastic response of the zirconia phase is modeled using the Arrenious power-law creep model and they assume that:

$$\dot{\varepsilon} = A\sigma^n e^{\left(-\frac{\Delta H}{RT}\right)} \qquad (1)$$

where the creep parameters A, n, and ΔH are given in Table 1 and R (the universal gas constant) is 8.317 J. $(\mathrm{mol.K})^{-1}$. They then focused on the stress relaxation that occurs for when X_2>1750μm (see Fig.1) and compared the stress distributions generated with the higher-order theory and the homogenized results.

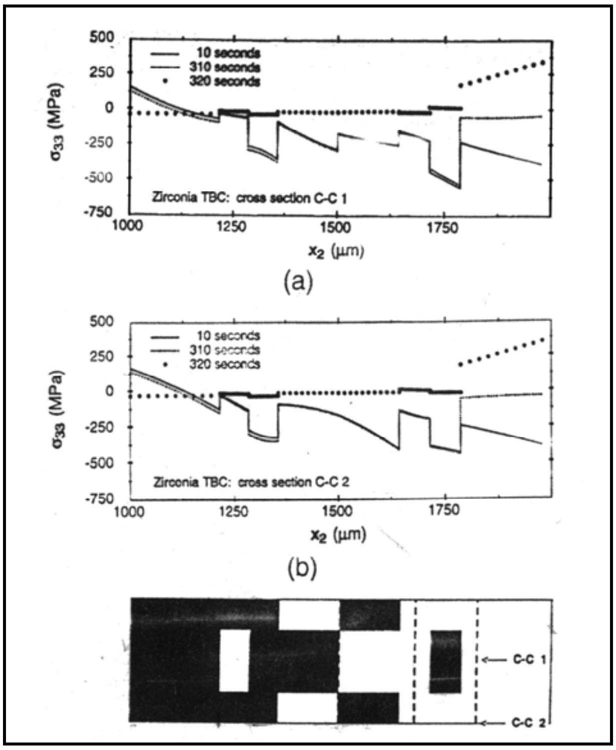

Fig. 1. Through-thickness normal stress distributions in the Zirconia-based functionally graded TBC with the coarsest microstructure at t=10, 310, and 320 s, predicted using the higher-order analysis by Arnold et al. [7] ((a) cross section C-C1 and (b) cross section C-C2)

3 Analysis Model

For thermal stress analysis of FGMs, material system, namely zirconia/CoCrAlY is considered. Zirconia as the ceramic phase at the TBC hot surface is exposed to an elevated temperature. In this paper, we consider isotropic elastic materials. The thermo-elastic material parameters of the individual constituents of the functionally graded TBC configurations are given in Table 1.

Material	Elastic Modulus, E(GPa)	Poisson's Ratio, ν	Thermal Expansion Coefficient, $\alpha(\times 10^{-6}\,K^{-1})$	Thermal Conductivity, $\kappa(W.(m.K)^{-1})$	A (Pa^{-n}/s)	n	ΔH (KJ/mol)
ZrO_2	36	0.20	8.0	0.50	1.89×10^{-6}	1.59	277
CoCrAlY	197	0.25	11.0	2.42	---	---	---

Table 1. Thermo-elastic and creep material parameters of the TBC constituents

The generic configuration of the investigated TBC is shown in Fig. 2. It consists of a pure ceramic layer at the upper surface that is exposed to a hot temperature and a pure CoCrAlY layer at the lower surface that is bonded to a steel substrate. The volume content of the CoCrAlY inclusions in the ceramic matrix gradually increases from the hot region to the cold region of the TBC such that halfway through the thickness of the TBC, the roles of the phases reverse and the CoCrAlY phase becomes the matrix phase below this point. Here, three TBC microstructures with different micro-structural refinement but the same overall content of CoCrAlY phase (shown in Fig. 3) in the order of increasing refinement numbers are considered. The coarsest micro-structure (Fig. 1(a)) consists of six distinct layers, whereas two other microstructures (Fig. 1(b) and Fig. 1(c)) consist of eight distinct layers. The outermost layers (layers 1 and 6) with the coarsest TBC microstructure are respectively pure ceramic and metallic layers whereas layers 2 and 5 contain one metallic and ceramic inclusion, respectively. Layers 3 and 4 are transition layers in which the roles of the inclusion and

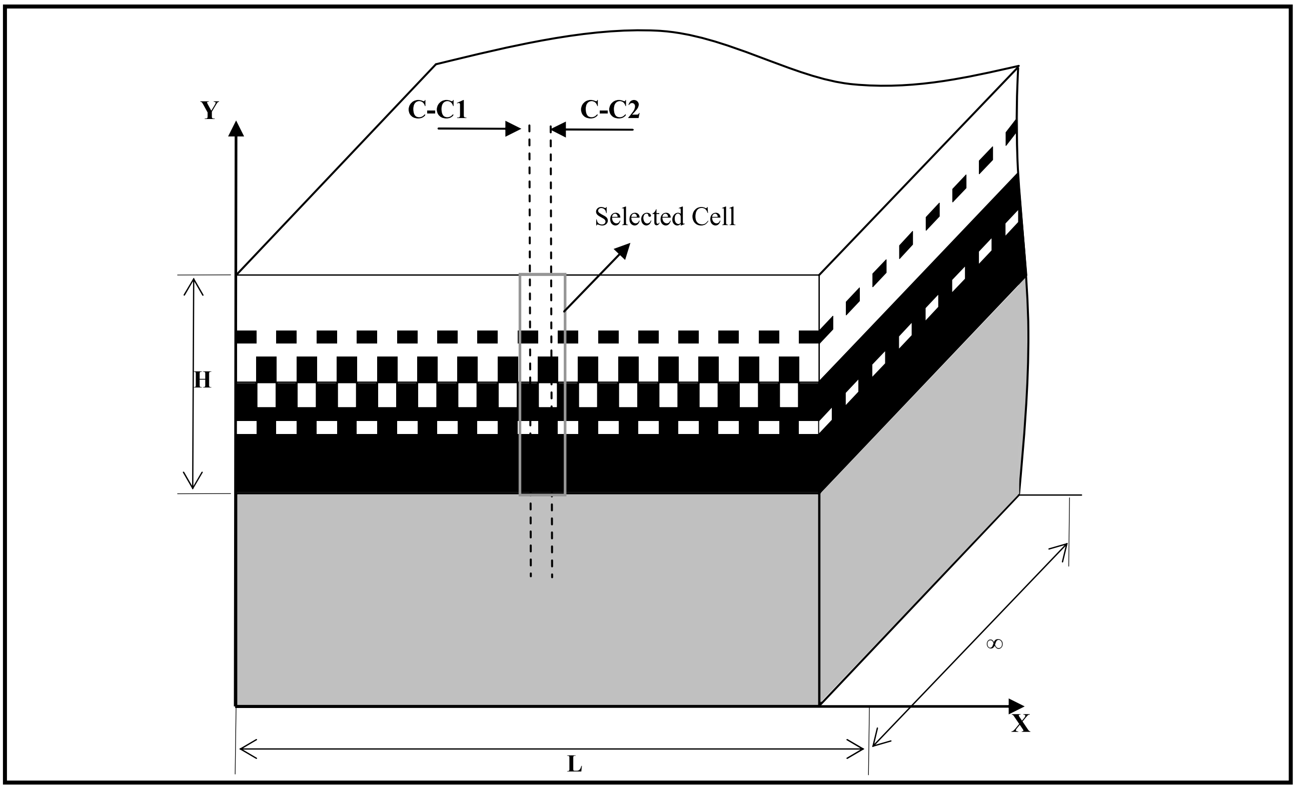

Fig. 2. Functionally graded zirconia/CoCrAlY TBC bonded to a steel substrate, the white regions represent the ceramic phase, the black regions represent the CoCrAlY phase, and the gray region represents the steel substrate.

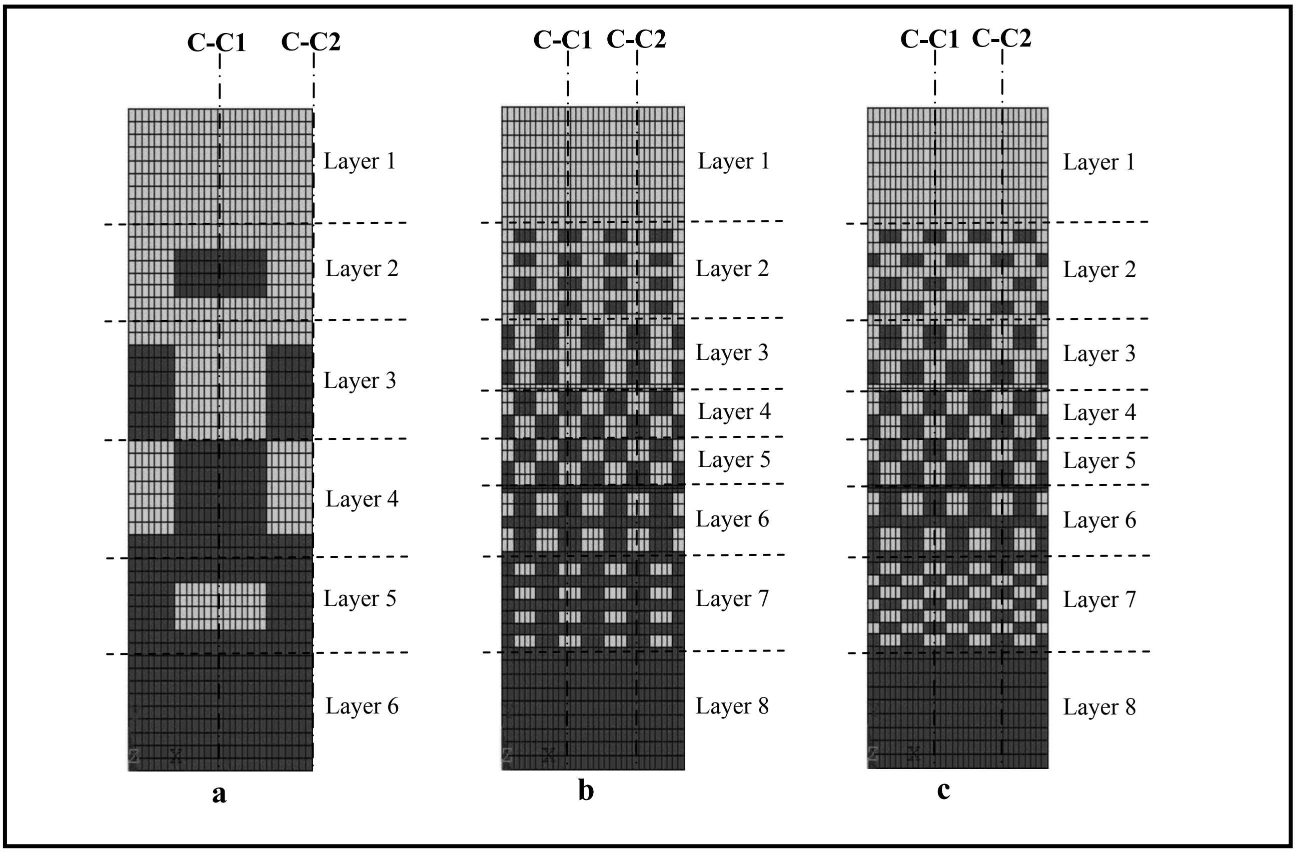

Fig. 3. TBC microstructures with different architectures and refinements

matrix phases reverse in a continuous manner, such that the metallic inclusion in layer 3, for instance, are in contact with the metallic matrix in layer 4, with a similar reversal for the ceramic phase. The eight layers of the two other microstructures are generated by subdividing each transition layer of the coarsest microstructure-layers 3 and 4- into two layers, while keeping the thickness of the remaining layers the same as in the coarsest microstructure. Subsequently, the inclusion dimensions in each layer are progressively decreased and the number of inclusions is appropriately increased, such that the inclusion volume fraction remains the same. Thus in these microstructures, the outermost layers, layers 1 and 8, are respectively pure ceramic and metallic layers while layers 2 and 7 and layers 3 and 6 contain similar number of metallic and ceramic inclusions, respectively. Layers 4 and 5 are transition layers. The difference between the two TBCs in Figs. 1(b) and 1(c) is the architecture of the inclusion phase in layers 2 and 3 and layers 6 and 7. In TBC of Fig. 1(b), the inclusion array in these layers is rectangular, whereas in TBC of Fig. 1(c), it is staggered. The staggered arrangement is more representative of actual stepwise functionally graded TBC microstructures in use today that exhibit random inclusion distributions, whereas the rectangular inclusion array in TBC of Fig. 1(b) is included for comparison purposes.

The above-described grading scheme produces a continuously graded microstructure with relatively large inclusion dimensions in the case of TBC of Fig. 1(a) (72 × 144 × 144(μm) platelike inclusions in layers 2 and 5 and 144 ×144 × 144(μm) inclusions in layers 3 and 4) and stepwise graded microstructures with substantially smaller inclusion dimensions in the case of TBC of Fig. 1(b) and 1(c) (18 ×36 × 36(μm) platelike inclusion in layers 2 and 7 and 36 × 36 × 36(μm) inclusions in layers 3 trough 6 of the TBC of Fig. 1(b) and 1(c)). The inclusion dimensions used in the TBC of Fig. 1(b) and 1(c) approach those that are used in practice. The inclusion dimensions of the coarsest microstructure are perhaps not realistic; however, the results obtained from this configuration will provide valuable information, in regard to the effect of micro-structural refinement and homogenization on the internal stress fields. The thickness (H) of the investigated TBCs is 1 mm, which is the same as the thickness of the steel substrate (see Fig. 1). This thickness is representative of functionally graded TBCs used in diesel-engine applications but not in turbine-blade applications, where TBC thickness dimensions up to 0.3-0.4 mm are typically used. The length (L) of the TBCs is sufficiently large so that the influence of the free edge on the internal thermo-mechanical fields calculated in the representative cross sections C-C 1 and C-C 2 (shown in Fig. 2 and 3 and located sufficiently far from the free edge) is negligible. This condition is ensured by imposing generalized plane-strain boundary conditions on the deformation of the microstructures shown in Fig. 2 in the Y-Z plane, as explained subsequently. Finally the depth is sufficiently large to be considered infinite.

We have also assumed that steady-state conditions prevailed and that no residual stresses were present at 25°C; the bottom surface was held at 25°C. The in-plane constraints imposed on the deformation of the entire configuration simulate the generalized plane strain in the Y-Z and X-Y planes. This deformation mode ensures that there is no bending about any of the axes and that plane sections in the Y-Z and X-Y planes remain planar.

Considering the shape of the cell and the symmetry of the problem, boundary conditions shown in Fig. 4 are chosen. These boundary conditions are common and logical. In these boundary conditions, side DC from the coating is completely constrained in the y-direction as shown in Fig. 4. Side AD is constrained in the x-direction, while it is free in the y-direction. And side BC is assumed to remain a vertical line; however the nodes on this line may all move together in the x-direction. Line AB is solely free. This set of boundary conditions shown in Fig. 4 is named BC1.

In order to analyze the stress distribution of the modeled cell, another set of boundary conditions named BC2 is considered. Although the assumption of such boundary conditions is not common in engineering problems, but the symmetry and the structure of the cells still remain logical while applying these boundary conditions. BC2 gives the modeled cell more freedom in deflection. In this set of boundary conditions, point D from the coating is completely constrained but other points of the side DC are constrained only in the y-direction as shown in Fig. 5. The two sides, AD and BC must remain straight parallel lines which can rotate together. Also, the considered cell of TBC can expand freely, as shown in Fig. 5.

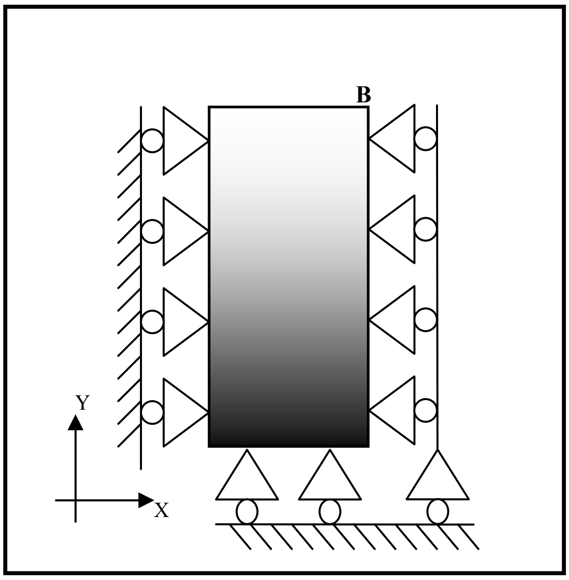

Fig. 4. Boundary conditions 1, for analysis of TBC a and b and c

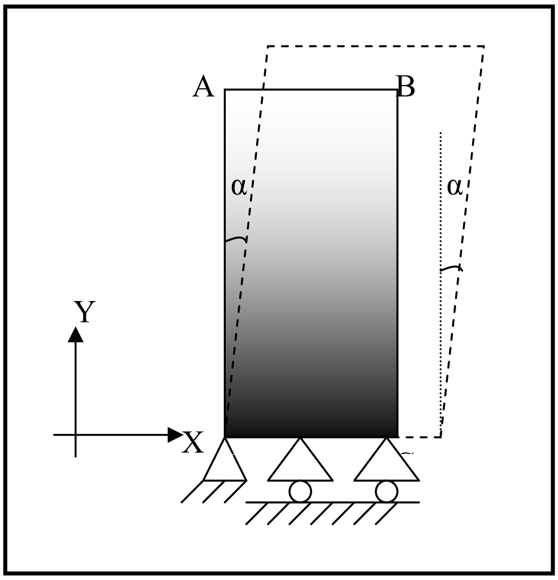

Fig. 5. Boundary conditions 2, for analysis of TBC a and b and c

In reality, thermal barrier coatings are loaded by thermal and mechanical loadings, simultaneously. Therefore, we investigate the stresses that appear in under the in-phase and out-of-phase thermal and mechanical loadings.

4 Results

The effects of the three microstructures of the functionally graded TBC on the internal thermal stress fields under thermal cyclic loadings were investigated. The thermal loading to which the top surface of the TBC subjected to was consisted of a ramp-up to 1200°C in 10 s, a saturation period of 300 s, and a ramp-down to 25°C in 10 s (Fig. 6).

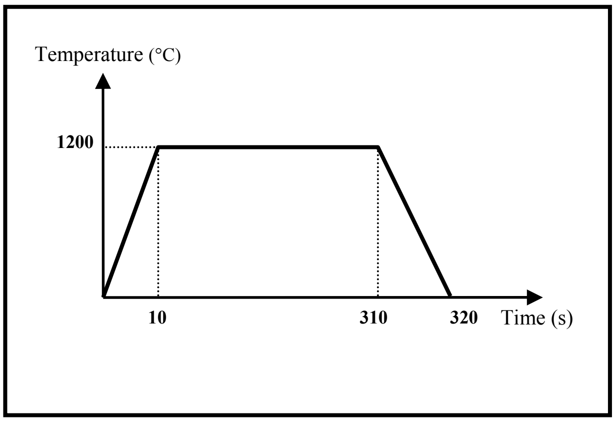

Fig. 6. Thermal loading history

Herein, we focus on the technologically important normal stress σ_x. Fig. 7 presents the corresponding normal stress distributions for the coarsest ZrO_2-based TBC microstructure carrying out BC1.

In this research work, because virtually no creep occurs in TBCs during the constant temperature period, when the top surface is exposed to 1200°C, the same distributions are obtained at t=10 and 310 s, as illustrated in Fig. 7.

Considering Fig. 7, we see that in layers 1, 2, and 3, compressive stresses and in layers 4, 5 and 6 tensile stresses appear in the model. In layer 2, we notice a step-like, sudden decrease in stress in cross section C-C 1. In layer 5, as seen in Fig. 7, normal stresses are tensile. Existence of tensile stresses in ceramic inclusion layer can cause internal cracks or debondings.

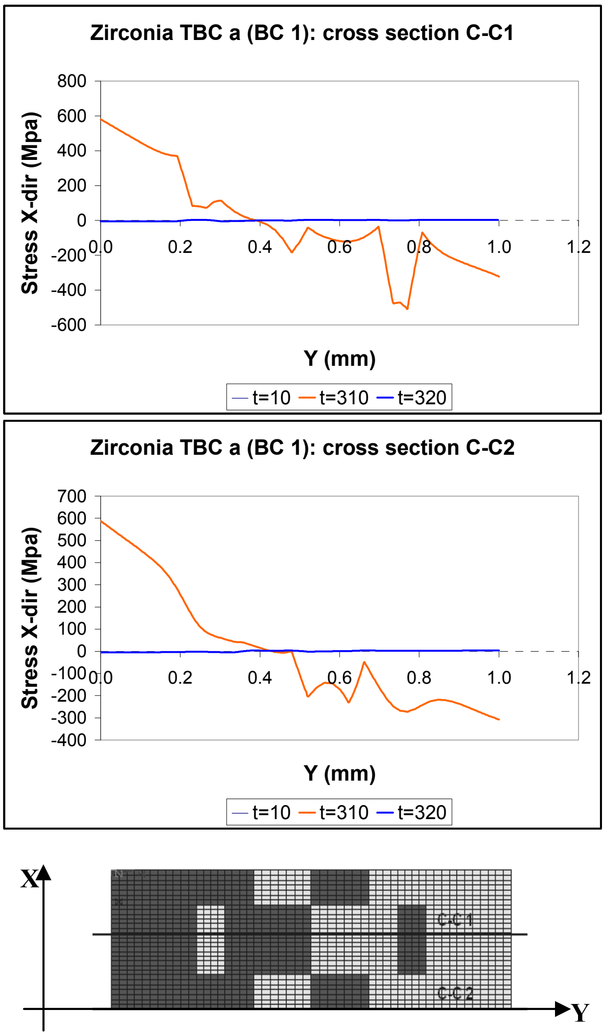

Fig. 7. Through-thickness X-dir stress distributions in the zirconia-based functionally graded TBC with the coarsest microstructure (TBC of Fig. 1(a) schematically shown at bottom of the figure) at t=10, 310, 320 s, carrying out BC1, predicted by the FEM method.

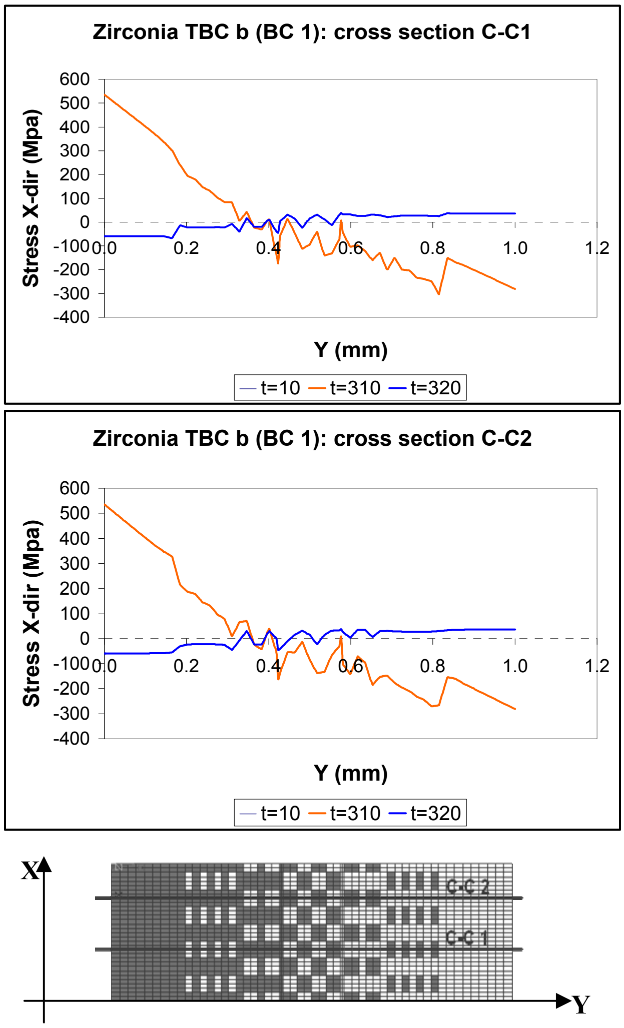

Fig. 8. Through-thickness X-dir stress distributions in the zirconia-based functionally graded TBC with the second microstructure (TBC of Fig. 1(b) schematically shown at bottom of the figure) at t=10, 310, 320 s, carrying out BC1, predicted by the FEM method.

In TBC of Fig. 1(b), the size of particles assumed for modeling is smaller and as mentioned before the results are closer to reality. Diagrams of normal stresses in x-direction for this TBC are shown in Fig. 8. Other assumptions of the problem are the same as the ones for the TBC of Fig. 1(a). As the micro-structural refinement continues, so does the frequency of stress oscillations due to the difference in thermo-elastic material parameters of the ceramic and metallic phases. The amplitude of stress in different layers dose not change when the refinement increases. Therefore, the common stress envelope could be useful in the design of functionally graded TBCs with different micro-structural scales.

Fig. 9 shows the variation of the x-direction stress in TBC of Fig. 1(c) at different times. Comparing Fig. 9 with Fig. 8, it can be concluded that the amplitude of stress oscillation is the same when the ceramic inclusions are arranged in a staggered array (as TBC c) and when they are arranged in a rectangular array (as TBC b).

In order to investigate the stress distribution in the cell with BC2, as for BC1, the thermal loading shown in Fig. 6 is considered. Fig. 10 presents the corresponding normal stress distribution for the coarsest ZrO_2-based TBC microstructure carrying out BC2. Considering Fig. 10 we see that compressive stresses appear in all layers of the model. As it will be discussed

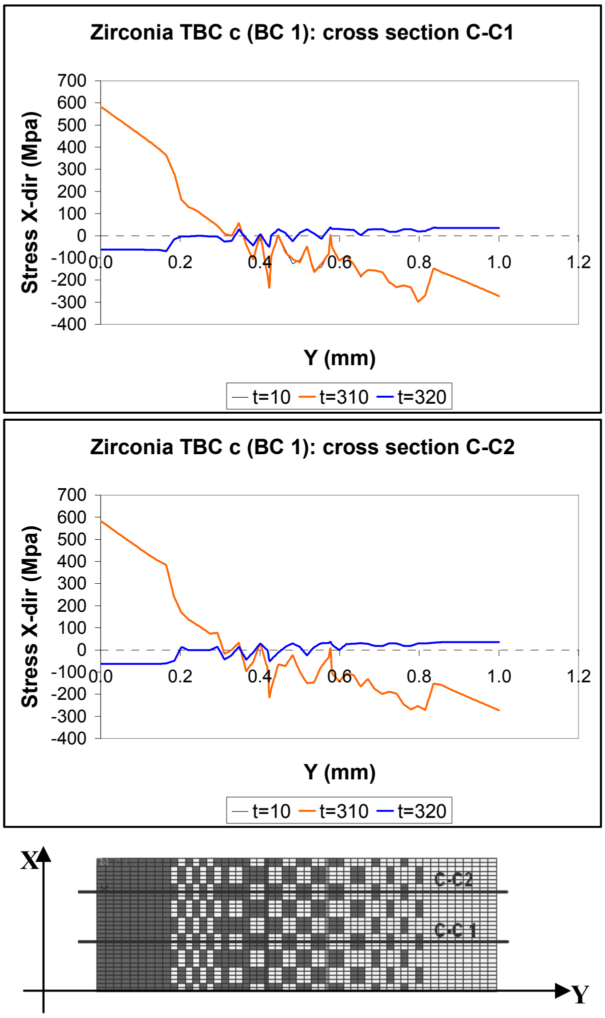

Fig. 9. Through-thickness X-dir stress distributions in the zirconia-based functionally graded TBC with the third microstructure (TBC (c) schematically shown at bottom of the figure) at t=10, 310, 320 s, carrying out BC1, predicted by the FEM method.

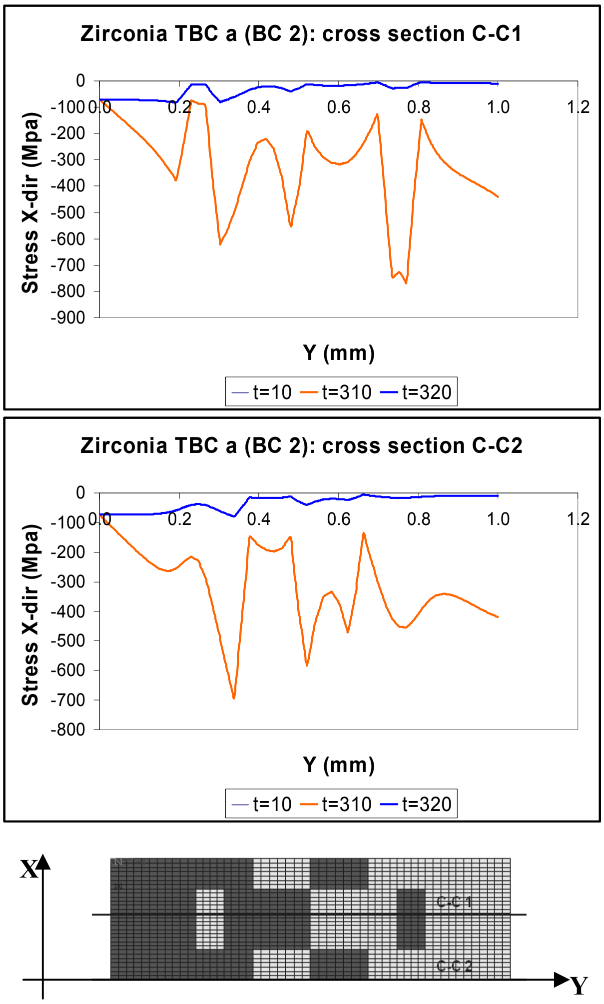

Fig. 10. Through-thickness X-dir stress distributions in the zirconia-based functionally graded TBC with the coarsest microstructure (TBC (a) schematically shown at bottom of the figure) at t=10, 310, 320 s, carrying out BC2, predicted by the FEM method.

Later, in this research work, if thermal and mechanical loadings are simultaneously applied to the TBC, then the stress distribution in Fig. 10 will displace. So, the mechanical loads play a dominant role on the stresses in TBCs. In layer 5, we notice a step-like sudden increase in stress in Fig. 10. However, the maximum normal stress appears in layers 1 and 5. These stresses can cause surface and internal cracks or debondings.

The in-phase thermal and mechanical loadings, as shown in Fig. 11, are applied to the modeled cell. Thermal loading is similar to the former loading and the mechanical loading to which the top surface of the TBC was subjected consisted of a ramp-up to 100 MPa in 10 s, a hold period of 300 s, and a ramp-down to zero in 10 s. By

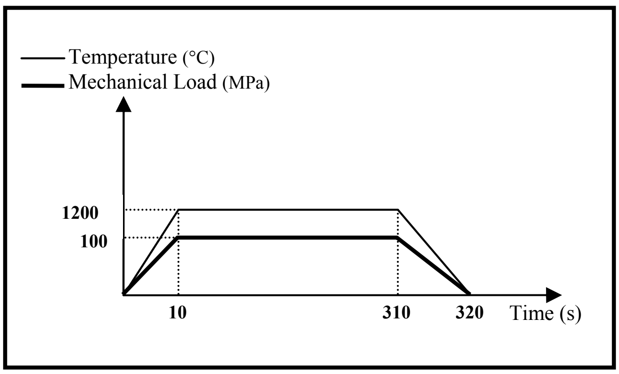

Fig. 11. The in-phase thermal and mechanical loading history

applying in-phase thermal and mechanical loadings to TBC 3, normal X-direction stresses appeared in the cell, are shown in Fig. 12. In Fig. 12, we see that if a constant mechanical loading be added to the thermal loading applied

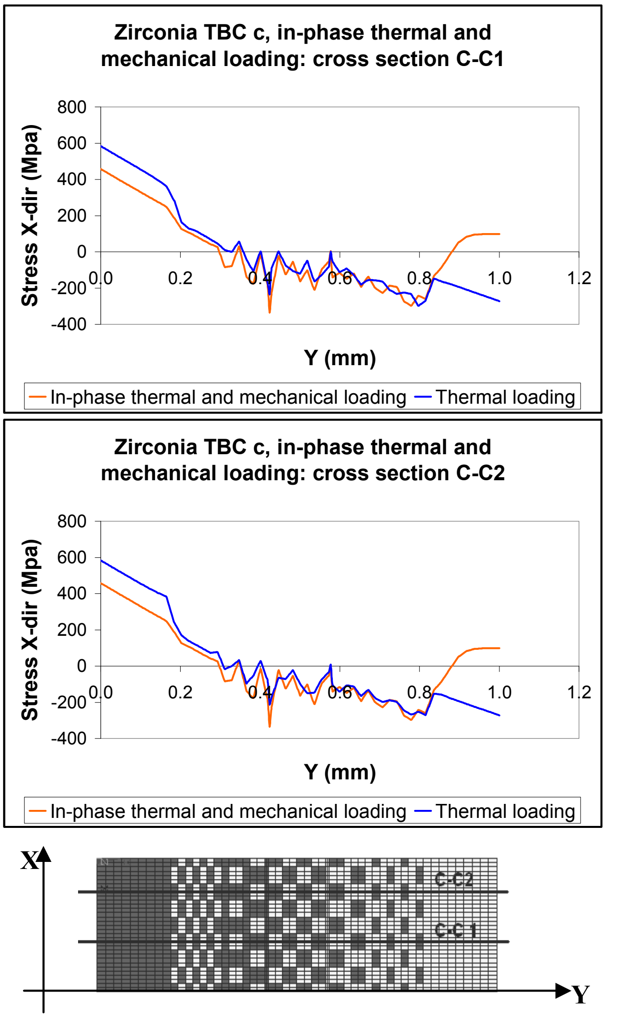

Fig. 12. Through-thickness X-dir stress distributions in the zirconia-based functionally graded TBC with the third microstructure TBC (c) loaded by in-phase thermal and mechanical loading, (schematically shown at bottom of the figure) at t=10, 310, 320 s, carrying out BC1, predicted by the FEM method.

to the TBC, the stress distribution will displace downward but the oscillations of the distribution remains unchanged. In layer 1, the stress in the

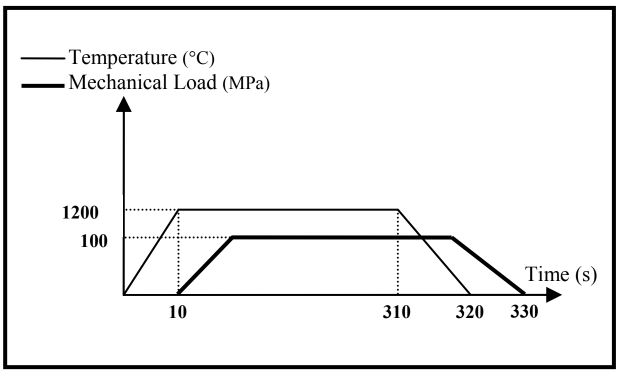

Fig. 13. The out-of-phase thermal and mechanical loading history

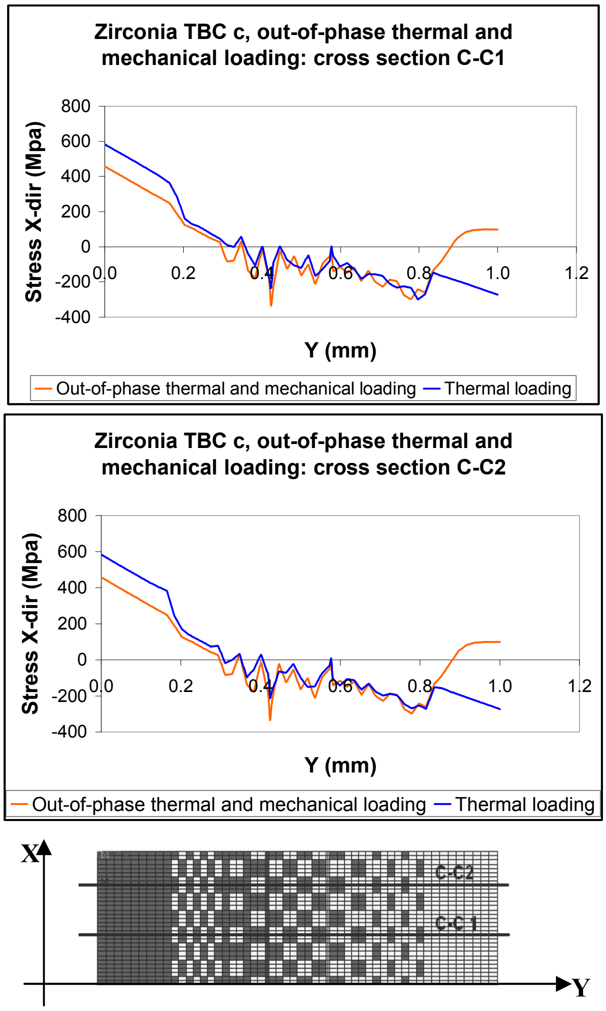

Fig. 14. Through-thickness X-dir stress distributions in the zirconia-based functionally graded TBC with the third microstructure TBC (c) loaded by out-of-phase thermal and mechanical loading, (schematically shown at bottom of the figure) at t=10, 310, 320 s, carrying out BC1, predicted by the FEM method.

in-phase thermal and mechanical loading is higher than the thermal loading; this happens because layer 1 is closer to the region where the mechanical loading is applied.

The out-of-phase thermal and mechanical loadings, as shown in Fig. 13, are applied to the modeled cell. The loading regime is similar to the former loading but the mechanical load is applied to the model with a 10 s delay. By applying this out-of-phase loading to the TBC of Fig. 1(c), the normal X-direction stresses will look like as shown in Fig. 14. It seems the delay with which the mechanical loading is applied, has no effect on the stress distribution at T=310 s in comparison with the in-phase loading.

5 Conclusion

The use of homogenization-based approach in the thermo-mechanical analysis of functionally graded thermal barrier coatings (TBCs) –like many macro-mechanical research works found in the literature [1-6]-obscures certain features of the microstructure-dependent stress distribution that may be important in regard to local failure mechanisms. To obtain more-detailed information on the local stress fields in functionally graded TBCs with different micro-structural scales requires the use of a computational approach that explicitly considers the interaction of the individual constituents, such as FEM used herein. This conclusion has been demonstrated by performing thermo-mechanical analyses of zirconia-based functionally graded TBCs that have been subjected to a cyclic through-thickness thermal gradient using the FEM. Three TBC configurations with the same overall volume fraction of the ceramic and metallic phases but different levels of micro-structural refinement have been considered. This includes a continuously graded TBC with a coarse micro-structure and stepwise graded TBCs with increasingly smaller inclusion dimensions in each layer, which are representative of the dimensions used in actual TBCs. The FEM analysis captures the oscillatory behavior of the stress field caused by the mismatch in the thermo-mechanical properties of the constituent phases. The amplitude and frequency of the stress oscillations are dependent on the extent of the property mismatch of the constituents and level of micro-structural refinement. The results suggest that for the stepwise functionally graded microstructures considered herein, additional micro-structural refinement in each layer would not change the magnitude of stresses in each layer. Thus, this common stresses could be useful in the design of actual, stepwise functionally graded TBCs with different micro-structural scales. Knowing the stress distribution in TBCs, we could investigate the failure mechanisms, which show that the normal tensile stresses in ceramic inclusion layers could cause internal cracks or debondings. The results also suggest that existence of tensile stresses in pure ceramic region can cause surface cracks in the thermal barrier coatings.

The existence of mechanical loading, in addition to thermal loading, affects the stress distribution in the TBCs and so should be considered in stress analysis of TBCs.

In this research work we neglected the creep effect during the investigation of the stress distribution in TBCs. However, we have already performed the FEM creep modeling of functionally graded TBCs, which the results will be published in a separate paper.

References

[1] Qianjun Xu and Shouwen Yu**.** Residual stress analysis of functionally gradient materials. *Mechanics Research Communications,* Vol. 26, No. 1, pp 55-60, 1999.

[2] Becker Jr, Cannon R M and Ritchie RO. An approximate method for residual stress calculation in functionally graded materials. *Journal of Mechanics of Materials*, pp 85-97, 2000.

[3] Woo J and Meguid S A. Nonlinear analysis of functionally graded plates and shallow shells. *Journal of Solid's Structures,* Vol. 38, pp 7409-7421, 2001.

[4] Lidong T and Wenchao L. Residual stress analysis of Ti-ZiO thermal barrier graded materials. *Journal of Materials and Design,* pp 627-632, 2002.

[5] Shen H S. Nonlinear bending response of functionally graded plates subjected to transverse loads and in thermal environments. *Journal of Mechanical Sciences,* Vol. 44, pp 561-584, 2002.

[6] Bahtui A and Eslami M R. Generalized coupled thermoelasticity of functionally graded cylindrical shells. *Journal of Numerical Methods in Engineering,* Vol. 69, pp 676-697, 2007.

[7] Pindera M, Aboudi J and Arnold S M. Thermomechanical analysis of functionally graded thermal barrier coatings with different microstructural scales. *J. Am. Ceram. Soc.*, 81 [6] 1525-36, 1998.

Copyright Statement